Development 136, 3121-3129 (2009) doi:10.1242/dev.033597

Receptor tyrosine phosphatases control tracheal tube geometries through negative regulation of Egfr signaling

Mili Jeon and Kai Zinn*

The formation of epithelial tubes with defined shapes and sizes is essential for organ development. We describe a unique tracheal tubulogenesis phenotype caused by loss of both *Drosophila* type III receptor tyrosine phosphatases (RPTPs), Ptp4E and Ptp10D. Ptp4E is the only widely expressed *Drosophila* RPTP, and is the last of the six fly RPTPs to be genetically characterized. We recently isolated mutations in *Ptp4E*, and discovered that, although *Ptp4E* null mutants have no detectable phenotypes, double mutants lacking both Ptp4E and Ptp10D display synthetic lethality at hatching owing to respiratory failure. In these double mutants, unicellular and terminal tracheal branches develop large bubble-like cysts that selectively incorporate apical cell surface markers. Cysts in unicellular branches are enlargements of the lumen that are sealed by adherens junctions, whereas cysts in terminal branches are cytoplasmic vacuoles. Cyst size and number are increased by tracheal expression of activated Egfr tyrosine kinase, and decreased by reducing Egfr levels. Ptp10D forms a complex with Egfr in transfected cells. Downregulation of Egfr signaling by the RPTPs is required for the construction of tubular lumens, whether extracellular or intracellular, by cells that undergo remodeling during branch morphogenesis. The *Ptp4E Ptp10D* phenotype represents the first evidence of an essential role for RPTPs in epithelial organ development. These findings might be relevant to organ development and disease in mammals, because PTPRJ (DEP-1), an ortholog of Ptp4E/Ptp10D, interacts with the hepatocyte growth factor receptor tyrosine kinase. PTPRJ corresponds to the murine *Scc1* (suppressor of colon cancer) gene.

KEY WORDS: *Drosophila*, Apicobasal polarity, Epithelial organ development, Phosphotyrosine signaling, Tracheae, Tubulogenesis

INTRODUCTION

Receptor-linked protein-tyrosine phosphatases (RPTPs) are single-span transmembrane receptors that reverse tyrosine phosphorylation events catalyzed by transmembrane or membrane-associated tyrosine kinases (TKs). Most RPTPs have extracellular (XC) domains that resemble cell adhesion molecules, suggesting that they interact with cell-surface or secreted ligands. *Drosophila* have six RPTPs, and mutations have been generated and analyzed for all of these. Five of the six were reported to be expressed only by central nervous system (CNS) neurons in late embryos. All published zygotic *Rptp* phenotypes are alterations in axon guidance or synaptogenesis (reviewed by Johnson and van Vactor, 2003; Jeon et al., 2008).

Type III RPTPs have single cytoplasmic PTP domains and XC domains that consist of long chains of fibronectin type III (FN3) repeats. There are five type III RPTPs in mammals. One of these, PTPRJ (DEP-1) is a tumor suppressor, encoded by the *Scc1* (susceptibility to colon cancer) locus in mouse (Ruivenkamp et al., 2002). A copy of *PTPRJ* is deleted in more than 50% of human colorectal, breast and lung tumors (Lesueur et al., 2005; Ruivenkamp et al., 2002). *C. elegans* has a single type III RPTP, DEP-1, which is a negative regulator of signaling through the worm Egfr ortholog LET-23 (Berset et al., 2005).

Drosophila has two type III proteins, Ptp4E and Ptp10D, which are closely related to each other (89% identity within the PTP domain) (Jeon et al., 2008; Oon et al., 1993). *Ptp10D* mutations alter axonal branching and fasciculation in the mushroom body (Kurusu and Zinn, 2008), and produce long-term memory deficits (Qian et al., 2007). Ptp10D works together with Ptp69D to control axon guidance across the CNS midline (Sun et al., 2000) and bifurcation of the SNa motor nerve (Sun et al., 2001).

We recently generated mutations in *Ptp4E*, which is the only broadly expressed RPTP in *Drosophila*. *Ptp4E* null mutants have no detectable phenotypes. However, when we made double mutants lacking both type III RPTPs, we observed that they die as early larvae, indicating that Ptp4E and Ptp10D compensate for the absence of one another during embryonic development. *Ptp4E Ptp10D* double mutants have subtle CNS axon guidance phenotypes, but these do not seem sufficient to produce lethality (Jeon et al., 2008). However, they do have severe tracheal defects that would prevent larval respiration.

The insect tracheal system is a network of tubes that transport oxygen to tissues. Tracheal tube walls are formed by a single layer of epithelial cells with apical surfaces that face the lumen. Tubulogenesis in the tracheal system involves cell migration, cell intercalation, lumen formation and lumen dilation. Mutations affecting lumen size and shape are found in genes encoding a variety of proteins, including septate junction proteins, chitin synthesis and modifying enzymes, and transcription factors. Some mutations cause increases in tube length that generate convoluted and serpentine branches, whereas others cause tubes to dilate in an uneven manner, producing cystic phenotypes (reviewed by Affolter and Caussinus, 2008; Swanson and Beitel, 2006). These mutations affect the lumen in all tracheal branch types.

In this paper, we show that loss of both type III RPTPs selectively alters lumen shape in branches that undergo cell shape change and cell junction remodeling during morphogenesis. The analysis of the double mutant phenotype provides new insights into tubulogenesis, and also demonstrates that lumen shape is controlled by signaling through the Egfr tyrosine kinase.

Broad Center, Division of Biology, California Institute of Technology, Pasadena, CA 91125, USA.

*Author for correspondence (zinnk@caltech.edu)

Accepted 2 July 2009

MATERIALS AND METHODS

Fly stocks and genetics

egfr^{k0511}, *egfr*^{f1}, *UAS*-Egfr-DN, UAS-phl-GOF, GFPn-lacZ/CyO, and UAS-mCD8-GFP were from the Bloomington Stock Center (Indiana University, Bloomington, IN, USA). UAS-dsRNA-Egfr was obtained from the VDRC (Vienna, Austria). UAS-Ptp4E-GFP has been described previously (Jeon et al., 2008). UAS-Egfr and UAS-Egfr^{Elp} (also known as Egfr^{E1}) were provided by J. Thomas (Salk Institute, La Jolla, CA, USA), and *btl*^{1187}, UAS-Btl-GAL4 and UAS-λBtl by M. Krasnow (Stanford University, Stanford, CA, USA). As previously described (Sun et al., 2000), rescue for Ptp10D was performed by crossing the GAL4 driver (*Btl-GAL4*, in this case) into *Ptp4E*^{1} *Ptp10D*^{EP1172}, which bears a UAS-containing P element upstream of the *Ptp10D* gene that causes a loss-of-function phenotype, because *UAS-Ptp10D* cDNA constructs do not rescue axon guidance phenotypes. To examine suppression and enhancement, *Ptp4E*^{1}*Ptp10D*^{1}*/FM7-GFP; Btl-GAL4* female flies were crossed to UAS-transgene male flies and progeny were examined for genetic interactions. All crosses were carried out at 25°C.

Immunohistochemistry

Whole-mount antibody staining of stage 15 embryos was performed using modified standard procedures (Jeon et al., 2008). The following primary antibodies were used: monoclonal antibody (mAb) 8B2 against Ptp10D (1:3), mAb DCAD2 against DE-cadherin [1:3; Developmental Studies Hybridoma Bank (DSHB)], mAb Cq4 against Crb (1:3; DSHB), mAb 2A12 (1:3, DSHB), and rabbit anti-GFP (1:1000; Invitrogen). Rabbit anti-Sas (1:1000) was kindly provided by D. Cavener (Vanderbilt University, Nashville, TN, USA), rabbit anti-Neurexin IV (1:2000) by H. Bellen (Baylor College of Medicine, Houston, TX, USA). Secondary antibodies used were: Alexa Fluor 488 and Alexa Fluor 568 (1:1000; Invitrogen), and HRP-conjugated goat anti-mouse IgG and IgM (1:300; Jackson). Embryos were mounted in Vectashield (Vector Laboratories) or glycerol. DIC images were photographed on a Zeiss Axioplan microscope (Carl Zeiss) using a 20×/0.5-0.17 Plan Neofluar objective. Fluorescence images were taken on a LSM510 Meta confocal laser scanning microscope (Carl Zeiss) using Plan-Neofluar 40×/1.3 Oil and Plan-Apochromat 63×/1.4 Oil objectives. Images were acquired using AIM software (Carl Zeiss) and processed using Adobe Photoshop.

Quantification of cyst phenotypes

Stage 15 embryos were stained with anti-Sas antibodies and dissected. Samples were imaged using confocal microscopy and *z*-stack projections were obtained. Measurements were made using ImageJ (NIH). Comparison of tracheal metameres (Tr 4-7) from ~10 mutant embryos showed little variation between hemisegments and thus measurements for all four hemisegments were pooled; at least five embryos were scored per genotype. All spherical enlargements along GBs were counted as cysts and diameters were measured. TC/LT branch junction diameter in mutants and in control embryos was measured at the widest section, across the TC branch immediately before bifurcation. For controls without GB cysts, two measurements were made at the thickest points of each GB.

Electron microscopy

Stage 15 embryos were dechorionated in bleach for 5 minutes and then fixed in a 1:1 mixture of heptane and 25% glutaraldehyde in phosphate buffer for 20 minutes. Embryos were manually devitellinized in electron microscopy (EM) fix buffer (2% formaldehye, 1% glutaraldehyde), then fixed in a 1:1 solution of EM fix buffer and 2% osmium tetroxide (OsO_4) at room temperature for 1 hour. Embryos were postfixed in 2% OsO_4 for 1 hour, dehydrated in an ethanol series, and embedded in Epon 812. Ultrathin sections (80 nm) were examined with a 120 keV T12 electron microscope (FEI Company) using a Gatan Ultrascan 2x2k CCD camera and Digital Micrograph image capture software (Gatan, Pleasanton, CA, USA).

Cell culture and immunoprecipitation

S2+ mtDer cells (from N. Perrimon, Harvard Medical School, Boston, MA, USA) stably expressing Egfr were maintained in 5 μg/ml puromycin (Calbiochem) in Schneider's media (Gibco) containing 10% fetal bovine serum (JRH Biosciences) and 1 U/ml penicillin (Gibco) and 1 μg/ml streptomycin (Gibco). Transfection of the Ptp10D full-length wild-type construct (Fashena and Zinn, 1997) or a full-length D→A substrate-trapping mutant construct (B. Burkemper and K.Z., unpublished) was performed according to the Effectene Transfection Protocol (Qiagen), and expression was induced with 500 μM $CuSO_4$. Cells were lysed in NP-40 cell lysis buffer (0.2% NP-40, 150 mM NaCl, 50 mM Tris-Cl pH 8.0, 1×protease inhibitor cocktail). Immunoprecipitation was carried out using rabbit polyclonal anti-Egfr serum (a gift from E. Bach, New York University, New York, NY, USA) or Ptp10D mAb 8B2. Samples were resolved on 7% SDS-PAGE gels, and western blots were carried out using rabbit anti-Egfr (1:10,000) or with a mixture of the anti-Ptp10D mAbs 8B2, 37F5 and 45E10 (ascites mix; each diluted 1:250). For immunoprecipitation using adult fly extracts, extracts were prepared by homogenizing 50 μl of adult flies (packed) with a Dounce homogenizer in an equal volume of lysis buffer (20 mM Hepes pH 7.6, 150 mM KCl, 1 mM DTT, 10% glycerol, 1% Triton X-100, 1×protease inhibitor cocktail) and then pelleting debris by centrifugation. Immunoprecipitation was carried out using mAb 8B2 and samples were resolved on 4-20% SDS-PAGE gels. Western blots were probed with a mixture of mAbs 8B2, 37F5 and 45E10.

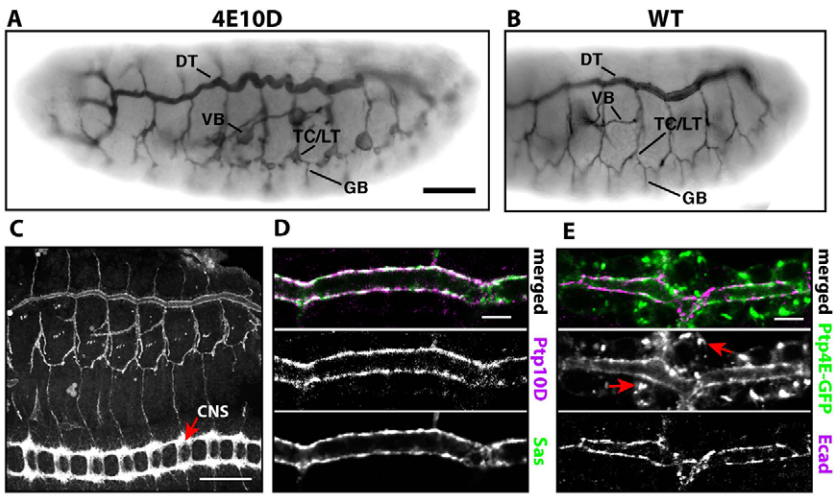

Fig. 1. Tracheal cyst phenotype in *Ptp4E Ptp10D* mutant embryos, and apical localization of Ptp10D and Ptp4E in tracheae. (**A**,**B**) Stage 15 *Ptp4E*^{1} *Ptp10D*^{1} (A) and wild-type (WT) (B) whole-mount embryos stained with the tracheal lumen marker antibody mAb 2A12, using HRP immunohistochemistry for visualization. Note that Fig. 6 shows that the 2A12 antigen (visualized by immunofluorescence) is reduced in *Ptp4E Ptp10D* unicellular tracheal branches relative to in wild type; however, we were still able to use 2A12 to visualize these branches using HRP immunohistochemistry. The HRP reaction can be carried out until saturation is reached, and under these conditions quantitative differences will not be detected; low and high-level expression will have the same appearance. (A) VBs and TC/LT branch junction cysts are indicated. Smaller cysts are found along LT branches and GBs. The middle section of the DT is convoluted. (**C-E**) Localization of Ptp10D and Ptp4E. (C) In stage 15 embryos, anti-Ptp10D mAb 8B2 labels the tracheae and the CNS axon ladder (arrow). (D,E) DT segments at stage 15. (D) Ptp10D (magenta) overlaps with the apical surface marker Sas (green). (E) UAS-Ptp4E-GFP (green), expressed in the trachea from Btl-Gal4, localizes to the apical membrane and overlaps with Ecad (magenta), which is apical in the DT. There are also bright Ptp4E-GFP spots on peripheral membranes (arrows). D and E are single confocal sections. Scale bars: in A, 40 μm for A,B; in C, 50 μm; in D,E, 5 μm.

RESULTS

Cysts form on unicellular and terminal tracheal branches in *Ptp4E Ptp10D* double mutants

Ptp4E Ptp10D double mutants died as hatched larvae with collapsed tracheae. When we examined tracheae in *Ptp4E Ptp10D* embryos, we observed large bubble-like cysts on select branches (Fig. 1A,B). Dorsal tracheal trunks (DTs) in double mutant embryos were serpentine, indicating that they had increased in length. However, the tracheal networks had normal branching patterns.

Earlier studies reported that Ptp10D is only expressed by neurons (Tian et al., 1991; Yang et al., 1991), but we found that newer mAbs made against native Ptp10D (Kurusu and Zinn, 2008) selectively stained the apical surfaces of all tracheal cells (Fig. 1C,D). The broadly expressed Ptp4E protein also localized to the apical membrane in tracheae (Fig. 1E).

To analyze the development of the cyst phenotype in *Ptp4E Ptp10D* mutants, we used confocal microscopy to examine dissected embryo 'fillets' stained for the apical membrane marker Crumbs (Crb) (Izaddoost et al., 2002), which localizes to the cysts. At stage 14, the junctions between the transverse connective (TC) and lateral trunk (LT) branches were enlarged (Fig. 2C). The anterior branches of the LT, which had not yet fused across segmental borders, had large cysts, and the ganglionic branches (GBs) had small cysts. By stage 15, cysts were observed at all TC/LT branch junctions and along the LT and GBs (Fig. 2D). The visceral branch (VB) also developed large cysts at this stage (Fig. 1A).

The genotype of the embryos shown in Fig. 2 is $Ptp4E^{1}$ $Ptp10D^{1}$, which bears two P element excision mutations that remove N-terminal coding sequence and are putative nulls. To confirm that the cyst phenotype is due to loss of RPTP expression, we examined embryos bearing four different combinations of mutant alleles (Fig. 3; see also Table S1 in the supplementary material). We quantitated the phenotype by measuring the diameter of the TC/LT branch junction and by counting cysts along the GBs. The average TC/LT branch junction diameter in stage 15 $Ptp4E^{1}$ $Ptp10D^{1}$ embryos was 8.4±0.5 μm (n=31), versus 2.8±0.1 μm (n=39) in wild-type controls. Hypomorphic double mutant combinations had intermediate TC/LT branch junction diameters. There were four to five cysts along each GB in all mutant genotypes; none was ever observed in wild type. The double mutant phenotype was fully rescued by tracheal-specific expression of either Ptp4E or Ptp10D from the Breathless (Btl)-GAL4 driver, showing that the RPTPs are required in tracheal cells and that they have equivalent functions (Fig. 3B-D). For all subsequent experiments, we used the $Ptp4E^{1}$ $Ptp10D^{1}$ mutant combination.

The tracheal system consists of tubes with different sizes and architectures (Fig. 2A,B) (Ghabrial et al., 2003). Multicellular tubes like the DT and the proximal portion of the TC branches have lumens surrounded by several cells that are separated from each other by intercellular junctions. Cysts were never seen on these branches. The branches that did have cysts were unicellular tubes with autocellular adherens junctions (AJs). These branches consist of cells arranged end-to-end that make tubes by rolling up and forming junctions with themselves. The lumen of such tubes is an extracellular compartment that is surrounded by the apical surface of a single cell. Cysts were also found in intracellular tubes, such as those of terminal cells in the lateral group branch (LG) (Fig. 2E), which are created by lumen formation within the cytoplasm of a cell. They are 'seamless' tubes, as they do not have cell junctions.

During formation of the tracheal branch network, terminal cells and cells in unicellular branches both undergo dramatic changes in shape. Terminal cells send out long cytoplasmic extensions and form fine-gauge tubes (also called tracheoles) within these extensions that deliver oxygen to individual cells. Branches with autocellular AJs are formed by a process of cell intercalation, in which cells shift their relative positions to transform from a paired to an end-to-end configuration (Ribeiro et al., 2004). During this rearrangement, intercellular junctions are replaced by autocellular junctions. By contrast, multicellular tubes grow in size, but the cells that compose these tubes do not undergo rearrangement or remodel their cell-cell junctions.

Cysts are apical compartments

To characterize cyst composition, we stained embryos for apical and basolateral markers. Crb and Stranded at Second (Sas) (Schonbaum et al., 1992) are apical membrane markers that appear as a single line in autocellular tubes, defining the path of the lumen (Fig. 4A). In mutants, both markers outlined the cysts (Fig. 4B,D). Two other markers secreted into the lumen or to the apical surface, 2A12

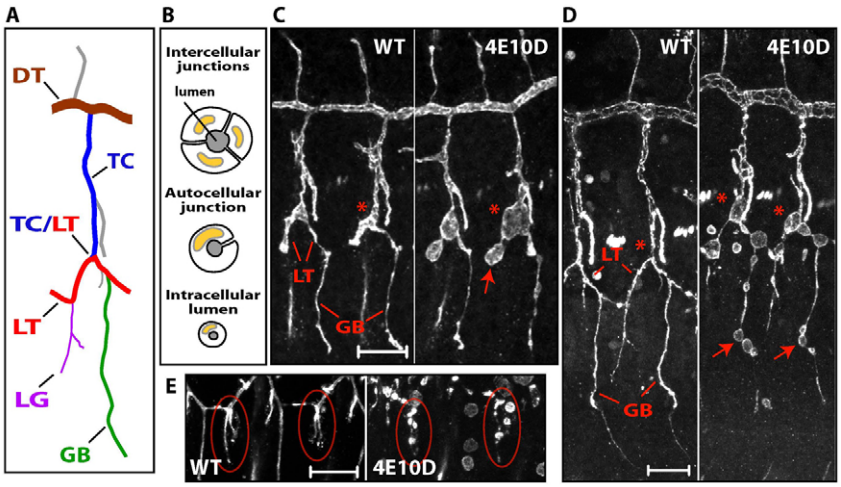

Fig. 2. Cysts are found only in unicellular and intracellular tubes. (**A**) Schematic representation of a tracheal metamer at stage 15. The branch names are labeled and color coded. (**B**) Cross-sections of tracheal tube types are diagrammed. Multicellular tubes consist of two or more cells surrounding the lumen. Unicellular tubes consist of a single cell wrapped around the lumen that forms autocellular junctions with itself. Intracellular tubes are composed of lumen within the cytoplasm; they lack cell junctions. DT and the proximal portion of TC are multicellular tubes, LG is an intracellular tube, and all other branches primarily consist of unicellular tubes with autocellular AJs. (**C**) Wild-type and $Ptp4E^{1}$ $Ptp10D^{1}$ dissected embryo fillets at stage 14, stained for the apical marker Crb. Two hemisegments are shown, with anterior to the left and dorsal up. In the mutant, the TC/LT branch junctions (asterisks) and the extending anterior branch of LT (arrow) are enlarged. (**D**) Wild-type and $Ptp4E^{1}$ $Ptp10D^{1}$ fillets at stage 15, stained for Crb. TC/LT branch junctions (asterisks) in the mutant have large cysts. GBs have 4-5 cysts per branch (arrows). (**E**) Cysts are found in LG terminal branches in the mutant. Two hemisegments are shown for wild-type and $Ptp4E^{1}$ $Ptp10D^{1}$ embryos, stained for the apical surface marker Sas. LGs are circled. Scale bars in C-E: 20 μm.

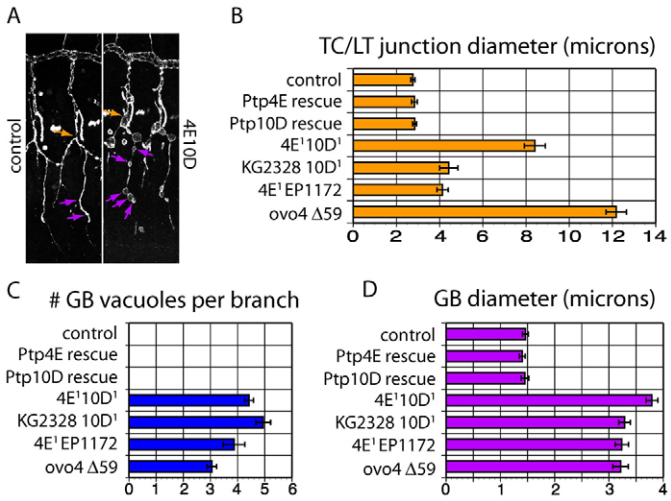

Fig. 3. Rescue of the phenotype by tracheal expression of Ptp4E or Ptp10D, and quantitation of cyst phenotypes in different genotypes. (**A**) Stage 15 embryo fillets were stained with anti-Sas to label the tracheae and imaged using confocal microscopy. Tr 4-7 were scored in stage 15 embryos. Measurements were made for the diameters of TC/LT branch junctions (orange arrow) and GBs (purple arrows). In control embryos (*Ptp4E*^{KG2328} *Ptp10D*^{1}/+), two measurements were made per GB, while in mutants all swellings on the branch were measured. (**B-D**) Expression of wild-type Ptp4E-GFP or Ptp10D in *Ptp4E Ptp10D* embryos fully rescued the cyst phenotype, as shown by all three bar graphs. There are no GB cysts at all in rescued or control embryos, so no bars are shown in the top three rows of C. All double mutant genotypes displayed similar phenotypes when GB cyst number and GB diameter metrics were evaluated. When TC/LT branch junction diameters were compared, *Ptp4E*^{1}*Ptp10D*^{1} and *Df(1)ovo4 Df(1)Δ59* showed larger measurements than the others. See Table S1 in the supplementary material for numerical data. The rescuing Ptp4E-GFP protein was expressed in tracheae and visualized in the experiment of Fig. 1. *Ptp4E* and *Ptp10D* alleles: *Ptp4E*^{1}, N-terminal coding sequences deleted; *Ptp4E (KG2328)*, P-element insertion; *Df(1) ovo4*, smallest deletion removing *Ptp4E*; *Ptp10D*^{1}, N-terminal coding sequences deleted; *Ptp10D (EP1172)*, P-element insertion; *Df(1) Δ59*, smallest deletion, removes *Ptp10D* and neighboring *bif*.

(Beitel and Krasnow, 2000) and Pio (Jazwinska et al., 2003), were also localized to cysts (Fig. 1A; data not shown). The basolateral membrane markers Neurexin IV (Nrx) (Baumgartner et al., 1996) and Coracle (Lamb et al., 1998), however, did not accumulate in cysts (Fig. 4C,D; data not shown). These results show that cysts are modified apical compartments.

When we visualized tracheal cells by expressing membrane-localized GFP (mCD8-GFP) with Btl-GAL4, we observed that GBs and terminal cell cysts were contained within cell boundaries (Fig. 4H,J). Cysts within terminal cells must be intracellular vacuoles, as they replace the Crb line that defines the path of seamless lumen within the cytoplasm. Cysts in unicellular branches, however, could either be vacuoles within cells or derivatives of lumen, which is extracellular in these tubes. To distinguish between these possibilities, we analyzed *Ptp4E Ptp10D* cysts at the ultrastructural level using transmission electron microscopy (TEM).

We examined horizontal sections through LT branches, which had the largest number of visible cysts (see legend to Fig. S1 in the supplementary material). In mutants, variable cyst diameters were observed, averaging around 4.6 μm (Fig. 5B,C; see also Fig. S1 in the supplementary material). In equivalent sections from wild-type embryos, lumen diameters in unicellular tubes were ~0.8 μm (Fig. 5A,D), which is consistent with published data (Beitel and Krasnow, 2000). Lumens in wild-type unicellular tubes were sealed by a single AJ, as expected (Fig. 5D). Many of the cysts in double mutants were associated with a single nucleus, suggesting that they were in unicellular tubes, and these also had single AJs (Fig. 5B,E). Some cysts had two AJs and two associated nuclei (Fig. 5C,F); these might be TC/LT branch junctional cysts, which were surrounded by multiple nuclei in confocal images (Fig. 4K). We did observe some cysts that had no visible junctions within the section plane, but we never saw cysts and normal lumen together in the same section.

The TEM data suggest that cysts in unicellular tubes are expanded forms of lumen sealed with AJs. To quantitatively evaluate the relationships between AJs and cysts, we examined embryos double-labeled for Crb and E-cadherin (Ecad), a key component of AJs. GBs in mutants usually had continuous Ecad lines, indicating that cell intercalation and junction exchange had occurred in a normal manner (Fig. 4F,M). Most GB cysts (85%; *n*=32 cysts) had a single line of Ecad staining bisecting the circular Crb-stained cyst outline (Fig. 4F,M, arrows). LT branch cysts, some of which are at TC/LT branch junctions where multiple tubes meet, had one (52%; *n*=21 cysts) or multiple (47%) Ecad lines traversing them (Fig. 4M, asterisks). These data, together with the TEM analysis, suggest that cysts in unicellular branches are usually associated with cell junctions, and therefore are modified forms of lumen rather than intracellular vacuolar compartments.

Lumens visualized by TEM in sections from double mutant embryos had less electron-dense material within them than did those in wild-type embryos (compare Fig. 5D to 5E,F). To examine luminal contents, we stained embryos for the luminal matrix antigen 2A12. We observed that 2A12 was reduced in unicellular branches of *Ptp4E Ptp10D* mutant embryos, but was present at normal levels in the multicellular DT and TC branches (Fig. 6). Thus, both the cyst and 2A12 accumulation phenotypes are restricted to unicellular and seamless tubes.

We used the mouse CD8-GFP marker to evaluate whether cell-cell interactions along tracheal branches were affected in *Ptp4E Ptp10D* double mutants. Cela and Llimargas described 'tissue integrity' defects in which connections between cells are thin or absent (Cela and Llimargas, 2006). We did not see such defects in *Ptp4E Ptp10D* embryos. Connections between cells had a normal appearance both at stage 14, when cysts first appear, and at stage 15, when they reach their maximum size (see Fig. S2 in the supplementary material). The tracheal network remained connected into stage 17 (data not shown).

Ptp4E and Ptp10D negatively regulate the Egfr tyrosine kinase in tracheal cells, and Egfr upregulation contributes to the cyst phenotype

RPTPs are regulators of TK signaling. To identify the TK(s) that is relevant to the *Ptp4E Ptp10D* phenotype, we expressed several activated TKs in tracheal cells of double mutant embryos. We observed dramatic effects for the Egfr^{E1} mutant protein (also known as Egfr^{Elp}), which has a single amino acid substitution that causes partial constitutive activation of the enzyme (Lesokhin et al., 1999). Egfr^{Elp} expression in wild type did not produce any cysts, but expression in the *Ptp4E Ptp10D* background caused TC/LT branch junction cysts to expand to an average diameter of 14.2±0.7 μm (*n*=31; Fig. 7B,D). It also caused cysts to appear on all dorsal branches (DBs), which are unicellular (Fig. 7B, arrows). Tracheal expression of wild-type Egfr produced a weaker phenotypical enhancement (Fig. 7D).

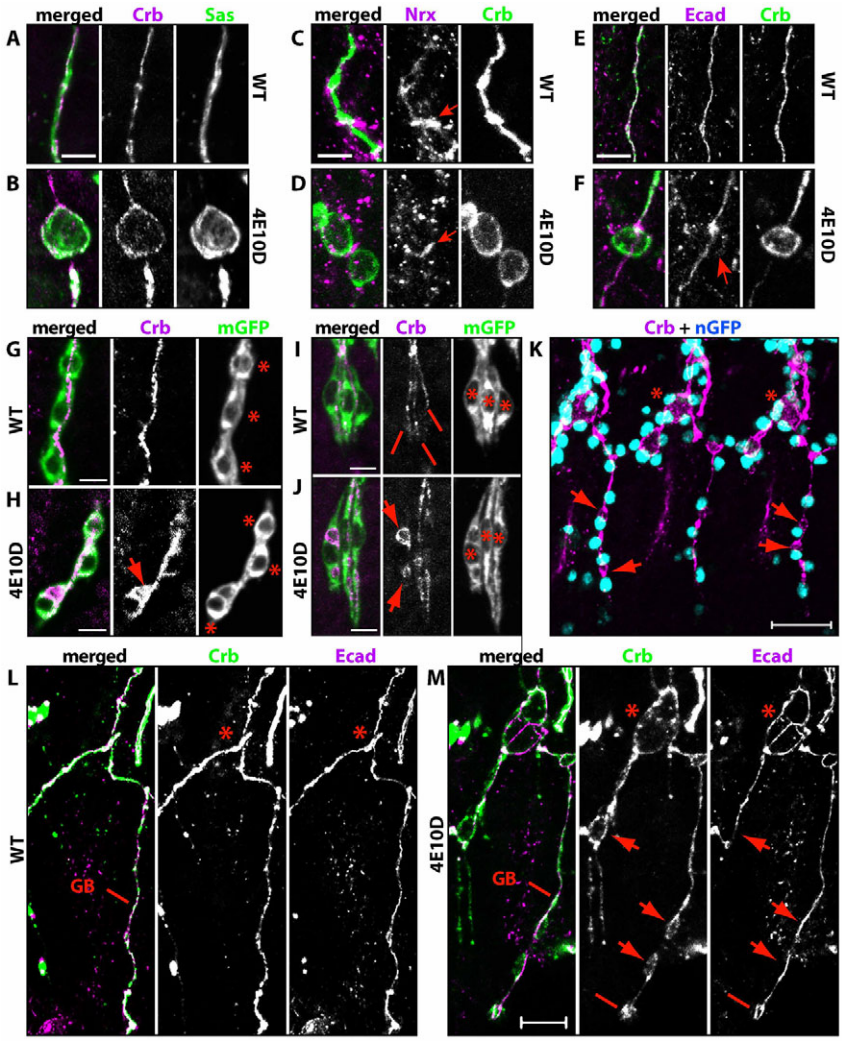

Fig. 4. Apical membrane markers accumulate in cysts. (**A-F**) GBs were labeled for apical markers Crb (A-F) and Sas (A,B), basolateral marker Nrx (C,D), and junctional marker Ecad (E,F). In wild type (A,C,E), apical and junctional markers label a line, and Nrx labels a thin line and the junction between adjacent cells in the branch (C, arrow). In *Ptp4E*^{1} *Ptp10D*^{1}, Crb and Sas are sequestered into the cyst (B), but Nrx is not (D). Ecad labels a line running through the cyst, indicating that an autocellular AJ is present; there is also weak labeling in the cyst that overlaps with Crb (F, arrow). (**G-J**) Membrane GFP (mGFP) was expressed in the tracheae and visualized with anti-GFP (green), together with anti-Crb (magenta) to label cysts. (G,H) Three cells in the GB are shown at high magnification (asterisks mark positions of nuclei). In wild-type (G), Crb localizes to the apical membrane and outlines the lumen, thus appearing as a line. In *Ptp4E*^{1} *Ptp10D*^{1} (H), a Crb-labeled cyst appears to be enclosed within the mGFP-labeled cell boundary (arrow). (I,J) High magnification views of three terminal cells (asterisks indicate nuclei), each of which forms an LG terminal branch, are shown. In wild type (I), lines indicate three cytoplasmic LG tubes. In *Ptp4E*^{1} *Ptp10D*^{1} (J), Crb labels cysts (arrows) located within the cell cytoplasm; the Crb lumen lines are missing in cells displaying cysts. (**K**) A *Ptp4E*^{1} *Ptp10D*^{1} stage 14 embryo expressing nuclear GFP (nGFP) in the tracheae was stained with anti-GFP (blue) and anti-Crb (magenta) antibodies. Cysts on GBs, indicated with arrows, are located adjacent to nuclei. At TC/LT branch junctions, cysts are surrounded by multiple nuclei (asterisks). (**L**,**M**) The TC/LT branch junction (asterisks) and the GB of a single hemisegment are shown in wild type (L) and *Ptp4E*^{1} *Ptp10D*^{1} (M), labeled for Crb (green) and Ecad (magenta). In the mutant, the TC/LT branch junction (M, asterisks) has multiple Ecad lines. Crb-labeled cysts in LT branches and GBs have normal Ecad lines running through them (M, arrows). Ecad also labels a ring-like structure (M, line) at the end of the GB. All panels are confocal *z*-stack projections. Scale bars: 5 μm in A-J; 20 μm in K; 50 μm in L,M.

The Btl receptor TK, which is an FGF receptor ortholog, controls branch extension in the tracheal system (reviewed by Affolter and Caussinus, 2008). Tracheal expression of λBtl, a constitutively dimerized version of Btl, also enhanced the *Ptp4E Ptp10D* phenotype, but to a lesser extent than did activated Egfr (Fig. 7D). Expression of two activated fly Src kinases had no effect (data not shown). Activated Raf (serine/threonine) kinase (Phl-GOF), which is downstream of Egfr in the canonical signaling pathway, also produced phenotypical enhancement (Fig. 7D).

Egfr is normally expressed in the tracheae, and is present on both the apical and the basolateral surfaces of tracheal cells (see Fig. S3 in the supplementary material). Egfr activity is required for tissue integrity (Cela and Llimargas, 2006). To determine whether a reduction in Egfr activity would suppress the cyst phenotype, implying that Egfr is an endogenous kinase regulated by RPTPs in tracheae, we reduced Egfr activity in the *Ptp4E Ptp10D* background in three different ways. We crossed in a single copy of an *Egfr* null mutation, *Egfr*^{k05115}. We also expressed

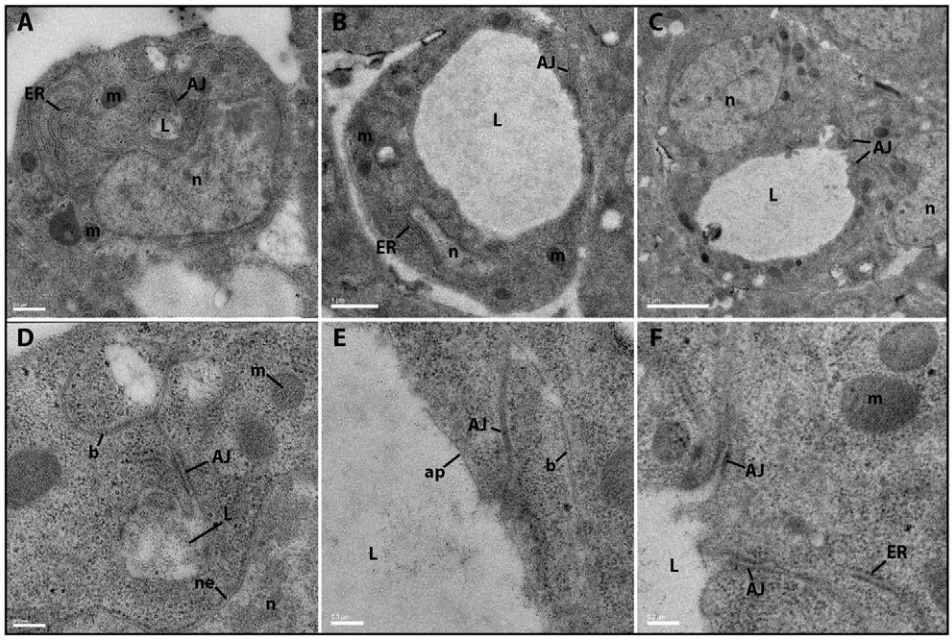

Fig. 5. TEM analysis shows that cysts are dilated lumens. Ultrastructural analysis of LT branch cross-sections in horizontal thin sections of stage 15 embryos was performed using TEM. (**A**) A wild-type tracheal branch with a single autocellular junction, and (**D**) a higher magnification view of the lumen and junction are shown. The AJ appears as a double electron-dense band between cell boundaries. The lumen contains diffuse electron-dense material. (**B**,**C**,**E**,**F**) *Ptp4E*^{1} *Ptp10D*^{1} tracheal branch cross-sections with a single autocellular junction and one nucleus (B,E), and with two cell junctions and two nuclei (C,F) are shown. The cyst in C,F is presumably at a TC/LT branch junction. E and F are higher magnification images of the lumen and junction areas in B and C, respectively. The lumens in mutant cells lack electron-dense material. Scale bars: 0.5 μm in A; 1 μm in B; 2 μm in C; 0.2 μm in D; 0.2 μm in E; 0.2 μm in F. n, nucleus; L, lumen; ER, rough endoplasmic reticulum; m, mitochondria; AJ, adherens junction; ne, nuclear envelope; b, basal membrane; ap, apical membrane.

an *Egfr* double-stranded RNA (RNAi) construct (Dietzl et al., 2007) and a dominant-negative (DN) Egfr mutant protein (Buff et al., 1998) in the tracheae. All three manipulations suppressed the phenotype. Egfr-DN and RNAi reduced the average diameter of the TC/LT branch junction in *Ptp4E Ptp10D* mutants from 8.4 μm to ~4 μm, whereas control embryos had junctions with an average diameter of 2.8 μm (Fig. 7D). Reduction of Btl kinase activity by crossing in a single copy of a *btl* mutation also produced statistically significant suppression, but the effect was less than that produced by removing a copy of *Egfr* (Fig. 7D). These data suggest that upregulation of Btl signaling contributes to the cyst phenotype, but that signaling through Egfr is the more important pathway for regulation of cyst formation.

We also attempted to evaluate whether Egfr is absolutely required for cyst formation by examining the phenotype of a triple mutant (*Ptp4E Ptp10D/Y, Egfr*^{k05115}*/Egfr*^{f1}) and comparing it to the *Egfr* transheterozygote. In *Egfr* mutants, tracheal development is severely impacted, and most branches do not form, thereby precluding a quantitative analysis of cyst size or number. However, we did observe some cyst-like structures on residual branches in the triple mutant (see Fig. S4 in the supplementary material), suggesting that cysts can still form when little Egfr activity is present. These cysts might be produced by an upregulation of Btl or other receptor TKs, as expression of activated Btl can enhance the cyst phenotype. We could not test whether Btl is required for cyst formation by examining *btl* triple mutant combinations, because loss of Btl abrogates tracheal branch extension.

C. elegans has a single type III RPTP, DEP-1, which is a negative regulator of signaling through the Egfr ortholog LET-23. A glutathione-S-transferase (GST)-DEP-1 cytoplasmic domain fusion protein bearing a 'substrate-trapping' (D→A) mutation in its active site was able to precipitate LET-23 from worm lysates (Berset et al., 2005). There are five mammalian type III RPTPs, one of which is DEP-1 (PTPRJ). A DEP-1 cytoplasmic domain fusion protein bearing a substrate-trapping mutant precipitated Met (hepatocyte growth factor receptor TK) from lysates of pervanadate-treated cells (Palka et al., 2003). Full-length mutant DEP-1 associated with a constitutively active CSF-1R (XC)-Met (cytoplasmic) receptor chimera in co-transfected cells, and wild-type DEP-1 could dephosphorylate the Met chimera.

These results suggest that type III RPTPs can interact with growth factor receptors, and therefore that there might be a direct interaction between Ptp10D/Ptp4E and Egfr. To test this idea, we used coimmunoprecipitation from transfected *Drosophila* Schneider 2 (S2) cells as an assay, as it provides a more rigorous demonstration of association than do GST pulldowns. To increase the probability of observing association, we transiently transfected *Ptp10D* expression plasmids into an S2 line that stably expresses Egfr from the inducible metallothionein (MT) promoter (Friedman and Perrimon, 2006). In this line, Egfr is expressed at high levels after copper induction and autoactivates, so that it does not have to be stimulated with a ligand. This has the advantage that, as in the studies with DEP-1 and the Met chimera (Palka et al., 2003), association with regulatory factors can be detected without the necessity to precisely time when the cells are lysed relative to when ligand is added. Egfr would be only transiently phosphorylated after ligand addition, and the timecourse of its interactions with regulatory phosphatases is unknown. However, Egfr dephosphorylation by the RPTP cannot be assayed in this line, as only a fraction of cells will express the RPTP, whereas all cells have activated Egfr.

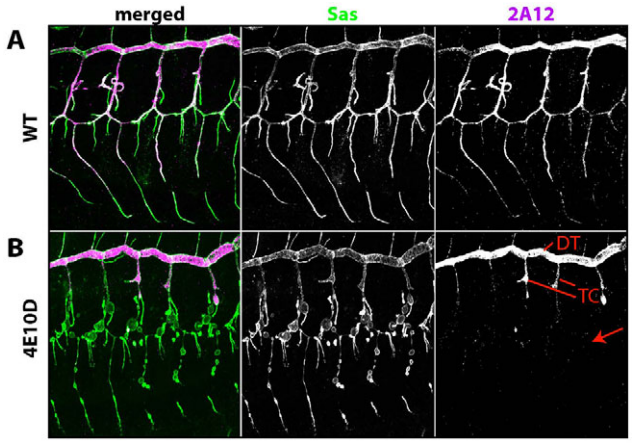

Fig. 6. The luminal 2A12 antigen fails to accumulate in *Ptp4E Ptp10D* tracheal branches that develop cysts. Stage 15 embryos were labeled for Sas (green) and the luminal marker 2A12 (magenta). (**A**) In wild-type control embryos, 2A12 accumulates in the lumens of all branches that are labeled with Sas. (**B**) In double mutant embryos, the 2A12 signal is absent or reduced in lumens of unicellular branches that develop cysts (arrow), but is present at wild-type or near wild-type levels in the multicellular DT and proximal TC branches.

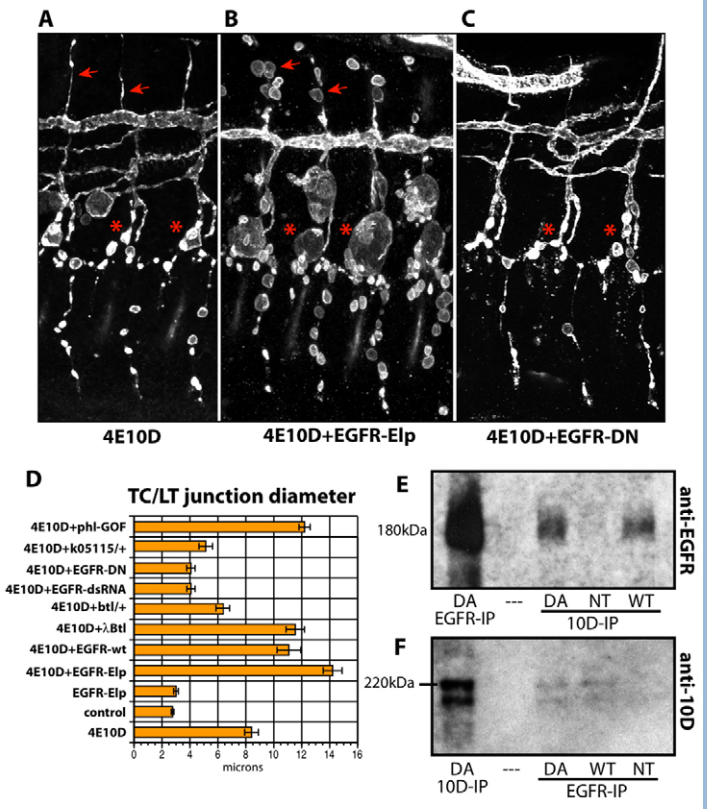

Fig. 7. Enhancement and suppression of the *Ptp4E Ptp10D* phenotype by Egfr constructs, and physical association between Ptp10D and Egfr. (**A-C**) Three hemisegments of stage 15 embryos stained for Sas are shown for (A) *Ptp4E*^{1} *Ptp10D*^{1}, (B) *Ptp4E*^{1}*Ptp10D*^{1}*; Btl-Gal4::UAS-Egfr*^{Elp}, and (C) *Ptp4E*^{1}*Ptp10D*^{1}*; Btl-Gal4::UAS-Egfr-DN.* (B) Constitutively activated Egfr^{Elp} expression in the tracheae causes dramatic enlargement of TC/LT branch junction cysts (asterisks). Almost all GB cells have cysts, and DBs, which have few cysts in unmodified mutants (<1 cyst/embryo) have many cysts (arrows) in the modified mutants. (C) Expression of dominant-negative Egfr partially suppresses the *Ptp4E*^{1} *Ptp10D*^{1} cyst phenotype. GBs show fewer cysts and TC/LT branch junction cysts are smaller than in *Ptp4E*^{1} *Ptp10D*^{1}. (**D**) Quantitation of the phenotypes. TC/LT branch junction diameters are increased relative to those of *Ptp4E*^{1} *Ptp10D*^{1} alone when Egfr^{Elp}, wt Egfr, activated Btl, or activated Raf (Phl) are expressed; they are decreased when Egfr signaling is reduced by using Egfr-DN or Egfr-RNAi, or by crossing in one copy of an *Egfr* or a *btl* mutation. Expression of Egfr^{Elp} in a wild-type background does not produce enlargement of the TC/LT branch junctions relative to wild-type controls. (**E**,**F**) Complex formation between Ptp10D and Egfr was detected by coimmunoprecipitation from lysates of copper-induced S2 cells stably expressing Egfr and transiently expressing wild-type or substrate-trapping mutant Ptp10D (both driven from the MT promoter). (E) Immunoblotting with anti-Egfr shows the 180 kDa Egfr band when anti-Egfr or anti-Ptp10D was used for immunoprecipitation from cells expressing wild-type or mutant (DA) Ptp10D. (F) Immunoblotting with anti-Ptp10D shows a doublet when anti-Ptp10D or anti-Egfr was used for immunoprecipitation from cells expressing wild-type or mutant (DA) Ptp10D. The upper band of the doublet is ~220 kDa, corresponding to the expected size of a glycosylated version of full-length Ptp10D, which is 1931 amino acids in length; these bands are not present in lysates from *Ptp10D* mutants (see Fig. S4 in the supplementary material).

We transfected S2-Egfr cells with MT promoter plasmids bearing wild-type or substrate-trapping mutant full-length Ptp10D, then induced Egfr and Ptp10D expression and immunoprecipitated Egfr or Ptp10D from cell lysates. We showed that the anti-Ptp10D mAb used for immunoprecipitation is specific for Ptp10D, as it does not precipitate the ~220 kDa Ptp10D doublet band from *Ptp10D*^{1} mutant lysates (see Fig. S5 in the supplementary material), and does not stain the CNS or trachea of *Ptp10D*^{1} embryos (Fig. S5 in the supplementary material). To detect Egfr, we used a well-characterized Egfr antiserum that others have employed for immunoprecipitation and blotting experiments in S2 cell lines (Vinos and Freeman, 2000; Ghiglione et al., 2002).

We observed that Egfr could be precipitated by anti-Ptp10D antibody from cells expressing wild-type or substrate-trapping mutant Ptp10D, and vice versa (Fig. 7E,F), demonstrating that the two proteins had formed a complex. In the studies of Palka et al., only mutant DEP-1 could co-precipitate the Met chimera (Palka et al., 2003). The chimera, however, lacks the Met XC domain; perhaps intact Met would have been able to stably associate with wild-type DEP-1.

DISCUSSION

In this paper, we analyze the phenotypes of *Drosophila* embryos lacking both type III RPTPs, Ptp10D and Ptp4E. Ptp10D regulates axon guidance in embryos and larvae (Sun et al., 2000; Sun et al., 2001; Kurusu and Zinn, 2008). It is selectively expressed on CNS axons and tracheal branches, and is apically localized in tracheal cells (Fig. 1).

Ptp4E is broadly expressed, and *Ptp4E* single mutants have no detectable phenotypes. The *Ptp10D/Ptp4E* gene pair was generated by a relatively recent duplication event, and the two proteins are closely related to each other. Although *Ptp10D* and *Ptp4E* single mutants are viable and fertile, double mutants die at the end of embryogenesis (Jeon et al., 2008). These data show that Ptp10D and Ptp4E have partially redundant functions during development. The lethality of the double mutants is due to respiratory failure that results from the malformation of tracheal branches.

The *Drosophila* tracheal system consists of a network of tubes with different sizes and architectures (Fig. 2) (Ghabrial et al., 2003). The larger tubes are multicellular, and have lumens surrounded by

several cells that are separated by intercellular junctions. Smaller tracheal branches are composed of unicellular tubes with autocellular AJs. The lumen of a unicellular tube is surrounded by the apical surface of a single cell, and is sealed by a longitudinal AJ. The smallest tubes, called tracheoles, are intracellular, seamless structures that form within the cytoplasm of terminal tracheal cells.

Loss of both type III RPTPs alters the shape of tracheal lumens, so that unicellular and seamless tubes develop large bubble-like cysts (Fig. 2). Multicellular tubes, however, are unaffected. This is a unique phenotype that has never been seen in any single mutant. The cysts are modified apical compartments, because they selectively incorporate apical but not basolateral cell surface markers (Fig. 4).

Cysts in seamless tubes are necessarily intracellular compartments. Cysts in unicellular tubes, however, are expanded segments of lumen, because they are associated with single AJs (Fig. 5). Accumulation of luminal matrix markers in unicellular tubes is reduced in double mutants, suggesting that they have a selective defect in lumen formation in certain tube types (Fig. 6).

RPTPs are regulators of tyrosine kinase signaling pathways. By examining the effects of manipulating tyrosine kinase activity on the cyst phenotype, we showed that the Egfr receptor tyrosine kinase is central to cyst formation (Fig. 7). Increasing Egfr activity enhances the cyst phenotype, while reducing Egfr suppresses it. The Btl (FGF receptor) tyrosine kinase also contributes to the phenotype. Egfr physically associates with Ptp10D in cultured *Drosophila* cells (Fig. 7).

Our data suggest that the phosphatases are negative regulators of Egfr signaling, and that the loss of this negative regulation is partially responsible for the cystic phenotype of *Ptp4E Ptp10D* double mutants. Cysts are not observed when activated Egfr ($Egfr^{Elp}$) is expressed in tracheae in a wild-type background, but we do not know if Egfr is activated to the same extent by the Elp mutation as it is by loss of the RPTPs. If it is, then excess tyrosine phosphorylation of RPTP substrates in other signaling pathways, perhaps including the FGF receptor pathway, might be required together with Egfr upregulation in order to produce the cyst phenotype.

Ptp10D and Ptp4E, which have catalytic domain sequences that are 89% identical, are likely to dephosphorylate the same targets, explaining why the phenotype is observed only when both RPTPs are absent. Ptp10D forms a complex with Egfr, and it is likely that the closely related Ptp4E would do so as well. Studies in mammalian cell culture have shown that the growth factor receptor tyrosine kinase Met can be dephosphorylated by the type III RPTP DEP-1, which is 50% identical to Ptp10D and Ptp4E within the catalytic domain (Palka et al., 2003). These findings, together with our genetic and biochemical analysis, suggest that autophosphorylated *Drosophila* Egfr might be a direct target for the enzymatic activities of Ptp10D and Ptp4E.

The fact that apical and luminal cell surface markers accumulate in cysts in unicellular and terminal branches, but not in multicellular branches, suggests that lumen formation in unicellular and terminal branches involves a common mechanism that is not required in multicellular tubes. This is odd, because the apical/luminal surface appears to be generated in a very different manner in unicellular and terminal branches. Lumen in unicellular branches is an extracellular compartment created by remodeling of the cell surface, whereas lumen in terminal branches is an intracellular compartment created by vesicular trafficking.

A possible solution to this conundrum is suggested by the observation that cells in multicellular branches increase in size during development but do not radically change their shapes. Cells in unicellular and terminal branches, however, undergo dramatic shape changes during branch outgrowth. These changes involve reorganization of the apical cell surface in unicellular branches, and the de novo generation of an apical compartment in terminal branches. In unicellular branches with autocellular AJs, the apical/luminal surface coordinates its growth with the remodeling of the cell as a whole, wrapping around the luminal matrix and forming a junction with itself. During elongation of terminal branches, apical surface and lumen markers are localized to growing lines within cells, indicating that lumen and its enclosing apical membrane form in synchrony with the extension of the rest of the cell.

We speculate that negative regulation of Egfr signaling by Ptp10D and Ptp4E is important for synchronizing apical membrane expansion with the remodeling of the rest of the cell. This could be mediated by phosphotyrosine-regulated interactions between the cytoskeleton and the apical membrane. In this context, it is interesting that loss of the *C. elegans* ERM (ezrin-radixin-moesin) homolog, which links the apical membrane to the underlying cortical actin network, causes cystic phenotypes in the intestine and the excretory canal (Gobel et al., 2004; Van Furden et al., 2004).

Acknowledgements

We thank Amin Ghabrial, Mark Krasnow, Sandra Schmid, Keith Mostov, Volker Hartenstein and members of the Zinn group for helpful discussions. We also thank Rosalind Young for help with TEM experiments; Alasdair McDowall and the Caltech EM Center for technical support; and Adam Friedman for help with mtDer cell culture. We also thank the Schuman lab for use of their confocal microscope, and Matthew Scott (Stanford) for providing laboratory space used for part of this work. This work was supported by an NIH RO1 grant (NS28182) to K.Z. Deposited in PMC for release after 12 months.

Supplementary material

Supplementary material for this article is available at http://dev.biologists.org/cgi/content/full/136/18/3121/DC1

References

Affolter, M. and Caussinus, E. (2008). Tracheal branching morphogenesis in Drosophila: new insights into cell behaviour and organ architecture. *Development* **135**, 2055-2064.

Baumgartner, S., Littleton, J. T., Broadie, K., Bhat, M. A., Harbecke, R., Lengyel, J. A., Chiquet-Ehrismann, R., Prokop, A. and Bellen, H. J. (1996). A Drosophila neurexin is required for septate junction and blood-nerve barrier formation and function. *Cell* **87**, 1059-1068.

Beitel, G. J. and Krasnow, M. A. (2000). Genetic control of epithelial tube size in the Drosophila tracheal system. *Development* **127**, 3271-3282.

Berset, T. A., Hoier, E. F. and Hajnal, A. (2005). The C. elegans homolog of the mammalian tumor suppressor Dep-1/Scc1 inhibits EGFR signaling to regulate binary cell fate decisions. *Genes Dev.* **19**, 1328-1340.

Buff, E., Carmena, A., Gisselbrecht, S., Jimenez, F. and Michelson, A. M. (1998). Signalling by the Drosophila epidermal growth factor receptor is required for the specification and diversification of embryonic muscle progenitors. *Development* **125**, 2075-2086.

Cela, C. and Llimargas, M. (2006). Egfr is essential for maintaining epithelial integrity during tracheal remodelling in Drosophila. *Development* **133**, 3115-3125.

Dietzl, G., Chen, D., Schnorrer, F., Su, K. C., Barinova, Y., Fellner, M., Gasser, B., Kinsey, K., Oppel, S., Scheiblauer, S. et al. (2007). A genome-wide transgenic RNAi library for conditional gene inactivation in Drosophila. *Nature* **448**, 151-156.

Fashena, S. J. and Zinn, K. (1997). Transmembrane glycoprotein gp150 is a substrate for receptor tyrosine phosphatase DPTP10D in Drosophila cells. *Mol. Cell. Biol.* **17**, 6859-6867.

Friedman, A. and Perrimon, N. (2006). A functional RNAi screen for regulators of receptor tyrosine kinase and ERK signalling. *Nature* **444**, 230-234.

Ghabrial, A., Luschnig, S., Metzstein, M. M. and Krasnow, M. A. (2003). Branching morphogenesis of the Drosophila tracheal system. *Annu. Rev. Cell Dev. Biol.* **19**, 623-647.

Ghiglione, C., Bach, E. A., Paraiso, Y., Carraway, K. L., 3rd, Noselli, S. and Perrimon, N. (2002). Mechanism of activation of the Drosophila EGF Receptor by the TGFalpha ligand Gurken during oogenesis. *Development* **129**, 175-186.

Gobel, V., Barrett, P. L., Hall, D. H. and Fleming, J. T. (2004). Lumen morphogenesis in C. elegans requires the membrane-cytoskeleton linker erm-1. *Dev. Cell* **6**, 865-873.

Izaddoost, S., Nam, S. C., Bhat, M. A., Bellen, H. J. and Choi, K. W. (2002). Drosophila Crumbs is a positional cue in photoreceptor adherens junctions and rhabdomeres. *Nature* **416**, 178-183.
Jazwinska, A., Ribeiro, C. and Affolter, M. (2003). Epithelial tube morphogenesis during Drosophila tracheal development requires Piopio, a luminal ZP protein. *Nat. Cell Biol.* **5**, 895-901.
Jeon, M., Nguyen, H., Bahri, S. and Zinn, K. (2008). Redundancy and compensation in axon guidance: genetic analysis of the Drosophila Ptp10D/Ptp4E receptor tyrosine phosphatase subfamily. *Neural Dev.* **3**, 3.
Johnson, K. G. and van Vactor, D. (2003). Receptor protein tyrosine phosphatases in nervous system development. *Physiol. Rev.* **83**, 1-24.
Kurusu, M. and Zinn, K. (2008). Receptor tyrosine phosphatases regulate birth order-dependent axonal fasciculation and midline repulsion during development of the Drosophila mushroom body. *Mol. Cell Neurosci*. **38**, 53-65.
Lamb, R. S., Ward, R. E., Schweizer, L. and Fehon, R. G. (1998). Drosophila coracle, a member of the protein 4.1 superfamily, has essential structural functions in the septate junctions and developmental functions in embryonic and adult epithelial cells. *Mol. Biol. Cell* **9**, 3505-3519.
Lesokhin, A. M., Yu, S. Y., Katz, J. and Baker, N. E. (1999). Several levels of EGF receptor signaling during photoreceptor specification in wild-type, Ellipse, and null mutant Drosophila. *Dev. Biol.* **205**, 129-144.
Lesueur, F., Pharoah, P. D., Laing, S., Ahmed, S., Jordan, C., Smith, P. L., Luben, R., Wareham, N. J., Easton, D. F., Dunning, A. M. et al. (2005). Allelic association of the human homologue of the mouse modifier Ptprj with breast cancer. *Hum. Mol. Genet.* **14**, 2349-2356.
Oon, S. H., Hong, A., Yang, X. and Chia, W. (1993). Alternative splicing in a novel tyrosine phosphatase gene (DPTP4E) of Drosophila melanogaster generates two large receptor-like proteins which differ in their carboxyl termini. *J. Biol. Chem.* **268**, 23964-23971.
Palka, H. L., Park, M. and Tonks, N. K. (2003). Hepatocyte growth factor receptor tyrosine kinase met is a substrate of the receptor protein-tyrosine phosphatase DEP-1. *J. Biol. Chem.* **278**, 5728-5735.
Qian, M., Pan, G., Sun, L., Feng, C., Xie, Z., Tully, T. and Zhong, Y. (2007). Receptor-like tyrosine phosphatase PTP10D is required for long-term memory in Drosophila. *J. Neurosci.* **27**, 4396-4402.
Ribeiro, C., Neumann, M. and Affolter, M. (2004). Genetic control of cell intercalation during tracheal morphogenesis in Drosophila. *Curr. Biol.* **14**, 2197-2207.
Ruivenkamp, C. A., van Wezel, T., Zanon, C., Stassen, A. P., Vlcek, C., Csikos, T., Klous, A. M., Tripodis, N., Perrakis, A., Boerrigter, L. et al. (2002). Ptprj is a candidate for the mouse colon-cancer susceptibility locus Scc1 and is frequently deleted in human cancers. *Nat. Genet.* **31**, 295-300.
Schonbaum, C. P., Organ, E. L., Qu, S. and Cavener, D. R. (1992). The Drosophila melanogaster stranded at second (sas) gene encodes a putative epidermal cell surface receptor required for larval development. *Dev. Biol.* **151**, 431-445.
Sun, Q., Bahri, S., Schmid, A., Chia, W. and Zinn, K. (2000). Receptor tyrosine phosphatases regulate axon guidance across the midline of the Drosophila embryo. *Development* **127**, 801-812.
Sun, Q., Schindelholz, B., Knirr, M., Schmid, A. and Zinn, K. (2001). Complex genetic interactions among four receptor tyrosine phosphatases regulate axon guidance in Drosophila. *Mol. Cell Neurosci.* **17**, 274-291.
Swanson, L. E. and Beitel, G. J. (2006). Tubulogenesis: an inside job. *Curr. Biol.* **16**, R51-R53.
Tian, S. S., Tsoulfas, P. and Zinn, K. (1991). Three receptor-linked protein-tyrosine phosphatases are selectively expressed on central nervous system axons in the Drosophila embryo. *Cell* **67**, 675-685.
van Furden, D., Johnson, K., Segbert, C. and Bossinger, O. (2004). The C. elegans ezrin-radixin-moesin protein ERM-1 is necessary for apical junction remodelling and tubulogenesis in the intestine. *Dev. Biol.* **272**, 262-276.
Vinos, J. and Freeman, M. (2000). Evidence that Argos is an antagonistic ligand of the EGF receptor. *Oncogene* **19**, 3560-3562.
Yang, X. H., Seow, K. T., Bahri, S. M., Oon, S. H. and Chia, W. (1991). Two Drosophila receptor-like tyrosine phosphatase genes are expressed in a subset of developing axons and pioneer neurons in the embryonic CNS. *Cell* **67**, 661-673.

Table S1. Quantitative analysis of the cyst phenotype

Genotype	TC/LT diameter (μm)	Number of cysts per GB*	GB diameter (μm)
ptp4E^{KG2328} ptp10D^{1}/+	2.8±0.1 (*n*=39)	0	1.5±0.1 (*n*=24)
ptp4E^{1} ptp10D^{1}	8.4±0.5 (*n*=31)	4.4±0.2 (*n*=31)	3.8±0.1 (*n*=167)
ptp4E^{1} ptp10D^{EP1172}	4.1±0.3 (*n*=24)	3.9±0.4 (*n*=23)	3.2±0.1 (*n*=89)
ptp4E^{KG2328} ptp10D^{1}	4.4±0.4 (*n*=36)	4.9±0.3 (*n*=35)	3.3±0.1 (*n*=173)
ptp4E$^{Df(1)ovo4}$ ptp10D^{Δ59}	12.2±0.5 (*n*=68)	3.0±0.2 (*n*=60)	3.2±0.1 (*n*=77)
ptp4E^{1} ptp10D^{EP1172}; Btl-GAL4	2.8±0.1 (*n*=35)	0	1.5±0.1 (*n*=24)
ptp4E^{1} ptp10D^{1}; Btl-GAL4>UAS-4E-GFP	2.8±0.1 (*n*=39)	0	1.4±0.1 (*n*=24)
Btl-GAL4>λBtl	3.1±0.2 (*n*=20)	0	–
ptp4E^{1} ptp10D^{1}; Btl-GAL4>λBtl	11.5±0.7 (*n*=32)	4.8±0.2 (*n*=31)	4.0±0.1 (*n*=150)
ptp4E^{1} ptp10D^{1}; btl^{1187}/+	6.3±0.5 (*n*=30)	3.6±0.4 (*n*=25)	2.7±0.1 (*n*=89)
Btl-GAL4>UAS-EGFR-Elp	3.0±0.2 (*n*=32)	0.2±0.1 (*n*=32)	1.8±0.1 (*n*=64)
ptp4E^{1} ptp10D^{1}; Btl-GAL4>UAS-EGFR-Elp	14.2±0.7 (*n*=31)	6.0±0.3 (*n*=31)	5.1±0.1 (*n*=185)
Btl-GAL4>UAS-EGFR-wt	2.9±0.1 (*n*=36)	0	–
ptp4E^{1} ptp10D^{1}; Btl-GAL4>UAS-EGFR-wt	11.1±0.8 (*n*=20)	5.4±0.3 (*n*=20)	4.3±0.1 (*n*=109)
ptp4E^{1} ptp10D^{1}; Btl-GAL4>UAS-dsRNA-EGFR	4.1±0.3 (*n*=45)	3.4±0.2 (*n*=42)	3.0±0.1 (*n*=143)
ptp4E^{1} ptp10D^{1}; Btl-GAL4>UAS-EGFR-DN	4.1±0.3 (*n*=72)	4.0±0.2 (*n*=58)	2.9±0.1 (*n*=233)
ptp4E^{1} ptp10D^{1}; Btl-GAL4>UAS-phl (GOF)	12.2±0.4 (*n*=51)	6.9±0.4 (*n*=32)	3.7±0.1 (*n*=220)
ptp4E^{1} ptp10D^{1}; egfr(k05115)/+	5.1±0.5 (*n*=36)	3.9±0.3 (*n*=36)	2.7±0.1 (*n*=141)

Tr4-7 were scored.
n is number of hemisegments scored.
*Number represents average number of cysts per full-length GB.